The genomic landscape of metallic color variation in ground beetles

Yi-Ming Weng[1,6]*, David H. Kavanaugh[2], Bryan Rubio-Perez[3], Jad Salman[3], Mikhail A. Kats[3,4,5], Sean D. Schoville[1]

1. University of Wisconsin-Madison, Department of Entomology, Madison, WI, USA
2. California Academy of Sciences, Department of Entomology, San Francisco, CA, USA
3. University of Wisconsin-Madison, Department of Electrical and Computer Engineering, Madison, WI, USA
4. University of Wisconsin-Madison, Department of Physics, Madison, WI, USA
5. University of Wisconsin-Madison, Department of Material Science and Engineering, Madison, WI, USA.
6. University of Florida, Florida Museum of Natural History, Gainesville, FL, USA

* Corresponding author: Yi-Ming Weng

Email:

weng22@wisc.edu

ORCID identifier:

Yi-Ming Weng: 0000-0002-8243-5061

David H. Kavanaugh: 0000-0001-8777-9771

Mikhail A. Kats: 0000-0003-4897-4720

Sean D. Schoville: 0000-0001-7364-434X

Abstract

The metallic color variation of beetles is a spectacular feature that has inspired diverse human cultures. However, little is known about the genetic basis of this trait or its ecological importance. In this study, we characterize the geographical distribution, optical mechanism, genetic basis, and ecological and evolutionary importance of metallic color variation in the *Nebria ingens* complex, an alpine ground beetle in the Sierra Nevada, California. We find that elytral color varies continuously across two allopatric species (from black *N. ingens* to green *N. riversi*), with hybrid populations showing intermediate coloration, and we demonstrate that the metallic color is generated from multilayer reflectors in the epicuticle of the elytra. By applying association mapping in natural populations (wild-GWAS) using high-density SNPs (1.2 million), we identify five promising candidate genes covarying with metallic variation, with known roles in cuticle formation and pigmentation pathways. Among these five genes, the gene *yellow*-like exhibits a heightened divergence pattern relative to the background genomic landscape and has been maintained despite gene flow. This finding, together with a significant correlation between color variation and water availability, suggests that metallic variation evolves as a local adaptation to environmental variation in the *N. ingens* complex.

Keywords: metallic color, Wild-GWAS, phenotypic evolution, functional ecology, *Nebria*, insects

Introduction

The impression created by bright metallic coloration in beetle wings is so stunning that diverse human cultures have used them in art and jewelry ('beetlewing art') for thousands of years (1, 2). This remarkable phenotypic trait is all the more impressive when its tremendous variation among beetles (order Coleoptera), a biodiverse group including more than 500,000 species, is recognized to have repeatedly evolved (3). The optical mechanism of metallic color in insects is well known, generated by the internal structure of the exoskeleton (4). In Coleoptera, the most prevalent internal structure is a multilayer reflector in the epicuticle or exocuticle, where the alternating electron dense and electron lucent layers reflect light in a specific range of wavelengths (3, 5). The thickness of the alternating layers strongly regulates the reflectance spectrum, with the longer peaked wavelengths generated from the thicker layers and vice versa (6). As a result of the discovery of the optical mechanism of metallic colors in insects, these microstructures have become an important resource for bioinspired materials (7-9).

Although metallic coloration is known to be polymorphic in numerous species (10, 11), little is known about the genetic basis of this phenotypic trait. Studies of many beetle species have shown that metallic color variation is typically additively determined by a small number of genetic loci (12-16), and only infrequently dependent on genotype-environment interactions (17). Compared to beetles, the genetic basis of metallic color in butterflies has been extensively explored. Both protein-coding and regulatory genes are known to control different types of microstructures on butterfly scales, which cause color reflection with different metallic hues (18, 19). However, the mechanisms of structural color formation in beetles and butterflies are fundamentally different. The reflectors of most beetles are embedded in the cuticle (except for some weevils and longhorn beetles), while the reflectors of butterflies usually form three-dimensional photonic structures on the wing surface (20-24). This difference implies independent evolutionary origins and

perhaps a novel genetic basis of metallic color in beetles. In this study, we use whole genome sequence data and association mapping in natural populations (wild-GWAS) to study metallic coloration of an alpine ground beetle. The *Nebria ingens* species complex is endemic to the Sierra Nevada in California, where it is found in the high elevation nival zone that is covered by snow throughout most of the year. Two species with divergent color in their elytra (appearing metallic green or black to human perception), *N. ingens* Horn and *N. riversi* Van Dyke, are geographically isolated, but form a broad admixture zone of intermediately colored individuals (25, 26) (**Figure 1**). The morphologically variable and genetically admixed populations make this species complex a great study system to apply wild-GWAS approaches (27, 28). Replicate admixed populations disrupt linkage disequilibrium across the genome, increasing power to isolate causative loci underlying the divergent phenotypes of the two species. Furthermore, the nearly continuous color variation improves the statistical power of association analyses. Leveraging this system, we identify candidates for the genetic basis of metallic color in beetles, as well as demonstrate a novel ecological function of metallic color variation, showing a strong correlation to the seasonal availability of water in nival habitats and the ability of different beetle phenotypes to retain water.

Results

Continuous variation and the mechanism controlling metallic color

We examined 368 beetles from 27 populations across the distribution of the species complex. In general, the reflectance spectra of green beetle elytra have a peak of 500 to 600 nm in wavelength, while beetles with black elytra have a decreased amplitude or complete loss of green wavelength reflectance (**Figure 1**). By converting the reflectance spectra to the CIELAB color space (L*a*b*) using the CIE standard illuminant D65, we found that many but not all beetles identified as *N. riversi* reflect a green hue, while most beetles identified as *N. ingens* or as hybrids reflect a dark green to black hue (**Figure 1**). The color variation is continuously distributed and thus likely to be a quantitative trait encoded by multiple genes (**Figure S1**).

From the elytral cross section, TEM images of green, dark green, and black elytra demonstrate variation in the inner epicuticle (cuticulin layer) (**Figure 2**), which is most pronounced in the green elytra (**Figure S2**). Here, there are 1-3 electron dense layers 50-100 nm thick (darker layers in the images due to reduced permeability for the electron beam), alternating with similar-width electron lucent layers, serving as a multilayer reflector. In the dark green elytra, only one electron dense layer is found, and no clear multilayer reflector was observed in the black elytra throughout the examined regions. Calculated spectra based on the thickness of the multilayer reflectors generally matches the visual color and observed spectra, with more alternating layers producing a stronger amplitude of light at a peak wavelength between 500 and 600 nm, roughly corresponding to green light from the elytra (**Figure S2**).

Color associated genes and their roles in color determination

Among the 1,237,702 scanned SNPs, 547 SNPs passed the adjusted *p*-value threshold at 0.001 in both ridge and lasso regression models (**Figure 3**), using a latent factor analysis adjusting for population structure. This candidate set intersects 156 genes, which were examined using gene ontology (GO) enrichment analysis (**Table S1**). A total of 65 biological process GO terms were enriched, including many cuticle-associated terms such as regulation of cuticle pigmentation (GO:0048079), melanin biosynthetic process (GO:0042438), ecdysone receptor-mediated signaling pathway (GO:0035076), and regulation of secretion (GO:0051046) (**Table 1**). However, these enriched terms are driven by a small number of cuticle formation genes from the intersected 156 genes, including *yellow*-like (*y*), *prophenoloxidase 2* (*ppo2*), two *ecdysone receptors* (*EcR*-1 and *EcR*-2), and *peroxidasin* (*pxdn*) (**Figure 3**).

Genetic divergence of color candidate genes

Pairwise population genetic divergence (F_{ST}) of the candidate genes, *yellow*-like, *prophenoloxidase 2*, and the two *ecdysone receptor* genes, were calculated, showing greater interspecific than intraspecific divergence when compared to intergenic and intragenic regions across the genome (**Figure S3**). For the *yellow*-like gene, the elevated

F_{ST} is found almost exclusively between populations across a known hybridization zone, and is more extreme than 98.1% of other genes that harbor more than 50 SNPs (**Figure 4**), or more extreme than 93.2% of all other genes (26). For *prophenoloxidase 2* and the two *ecdysone receptor* genes, extreme values of F_{ST} are only found between the northernmost population (i.e., Conness Lake) and the admixed populations in the southern contact zone (**Figure S3**).

Correlation between color variation, water loss rate, and SWE

To test the physiological and ecological function of metallic color, we performed pairwise correlation analysis using color variation (axis a*), water loss rate, and seasonal water availability in the nival zone (represented by measurements of snow water equivalent, SWE) (**Figure 5**). The results showed a significant negative correlation between beetle color and SWE (ρ=-0.37, p=4.2e-13, 95% CI=-0.46 to -0.26), with greener hues occurring in more snow-rich habitats, and a significant positive correlation between water loss rate and SWE (ρ=0.32, p=0.011, 95% CI=0.07 to 0.53). We also found a negative trend between color variation and water loss rate that was nearly significant (ρ=-0.22, $p=0.09$, 95% CI=-0.46 to 0.04), suggesting that greener elytra may be linked to faster water loss over time.

Discussion

Despite a long-standing interest in the metallic color of insects, distinct knowledge gaps in our understanding of color variation remain. Beyond the lack of knowledge for the most biodiverse animal group, the beetles, gaps include the nebulous genetic basis and the unknown ecological importance of metallic color variation. By applying wild-GWAS to an alpine ground beetle species complex with admixed populations, we found promising candidate genes that are statistically associated with the metallic variation generated from multilayer reflectors in the epicuticle and functionally involved in cuticle formation and pigmentation. We also found that an absence of green metallic color in the *N. ingens* complex is positively correlated with water loss resistance, where black colored beetles are found in drier and warmer nival regions. Finally, heightened interspecific genetic

divergence of the candidate gene *yellow*-like near a historical contact zone implies that population genetic differences are maintained by selection in the presence of gene flow.

Genetic basis of the metallic color in the N. ingens complex

Color variation can be categorized by optical mechanism, which varies across insect lineages (3). For instance, in Coleoptera, iridescent color generated by three-dimensional photonic structures has been found in weevils and longhorn beetles, whereas multilayer reflectors are widespread in distantly related lineages of jewel beetles (Buprestidae), ground beetles (Carabidae), leaf beetles (Chrysomelidae), and scarab beetles (Scarabaeidae) (29). Although the structural layering may be common to the ancestor of beetles, structural coloration has been repeatedly gained, lost and modified (29). Yet, very little is known about how genetically complex this phenotypic variation is across beetles.

In this study, we found that a multilayer reflector is responsible for the metallic color variation of the *N. ingens* complex. This is directly supported by the presence of the periodically alternating electron dense and electron lucent layers in the epicuticle, with their estimated reflectance spectra matching the elytral colors and the observed spectra (**Figure 2**). Such resemblance of the calculated and observed reflectance spectra has been used to determine the optical mechanism of metallic color in many other insects (6, 30-35). In the *N. ingens* complex, the high amplitude peak between 500 and 600 nm in the reflectance spectrum is directly correlated with the number of alternating layers in the epicuticle. This type of color variation, with varying amplitude at certain wavelengths due to differing numbers of layers with the same thickness, is structurally different from a type of variation where the reflectance peak shifts to different wavelengths due to differing layer thickness, and thus should be considered as a separate type of color variation. In nature, the type of color variation seen in *N. ingens* seems to be less common but has been reported in different beetle families (16, 36, 37).

The genetic variation that underlies the arrangement of multilayer reflectors (i.e., layer count and thickness) is still unexplored. Because the cross-sectional anatomy of the multilayer reflector is relatively conserved over several phylogenetically distant lineages, the trait is likely to be homologous. In this study, we identified numerous SNPs that

significantly covary with the color variation in the *N. ingens* complex. From the 156 candidate genes, we found enriched functions that alter cuticular profiles through the tyrosine-based cuticle sclerotization and pigmentation pathway (**Figure 3**), a vital biochemical pathway altering the insect cuticle profile by converting tyrosine into pigments (e.g., melanin and dopamine-melanin) (38, 39). The candidate genes include *yellow*-like, *prophenoloxidase,* and *peroxidasin*. Yellow protein (i.e. dopachrome conversion enzyme, DCE) from the *yellow* gene family advances melanin biosynthesis (38). This gene was previously found to mediate the melanin biosynthesis process in *Drosophila*, flour beetles (*Tribolium*) and the assassin bug (*Platymeris biguttatus*) (40-44). Prophenoloxidase can be activated into Phenoloxidase (45, 46) to convert tyrosine to 3,4-dihydroxyphenylalanine (DOPA) in the tyrosine-based cuticle pigmentation metabolic pathway. Finally, Peroxidasin is involved in extracellular matrix formation including protein crosslink sclerotization (47). However, both Prophenoloxidase and Peroxidasin have been reported as responding to wounding and encapsulation, with little information regarding their function in regulating cuticular properties (47-49). Our list of enriched functions also includes the ecdysone receptor-mediated signaling pathway, which modulates the developmental patterning of insects during morphological transitions. Ecdysone receptor (*EcR*) is an important nuclear hormone receptor that induces cuticle remodeling during metamorphosis. In many butterfly species, *EcR* has been found to determine the color pattern of the eyespots on the wings. In termites, *EcR*-knockdown results in the reduction of expression levels of the *laccase2* gene (a key phenoloxidase gene in cuticle melanization and tanning) and thinner pigmented layers in the cuticle that lead to paler soldier termites (50, 51).

In the *N. ingens* complex, black elytra are most likely formed as a result of a lack of alternating electron dense and electron lucent layers in the epicuticle (**Figure 2C**). Because these layers are formed by the accumulation of melanized lamellae in the cuticle, we propose that the candidate genes involved in cuticle sclerotization and pigmentation pathway modify the development of multilayer patterning. Although several gene silencing experiments have successfully identified the cuticle pigmentation gene in the tyrosine hydroxylation pathway in insects, how these genes relate to the formation of the multilayer

reflector remains unexplored. The genes identified in our wild-GWAS approach provide strong candidates for future developmental and functional genetic experiments to test the genetic basis of metallic color generated by multilayer reflectors in the cuticle.

The evolutionary and ecological role of metallic color in the N. ingens complex

The ecological function of metallic color has been considered an important characteristic in biotic interactions, both within and between species. In beetles, sexual selection, mimicry, camouflage, or aposematism are widely accepted functions for metallic color (52-57). But just how relevant biotic interactions are for the diversity of color patterns in beetles remains unclear. Other studies have shown that metallic color may instead result from adaptation to abiotic environmental factors (17, 58, 59). In particular, the cuticular components associated with desiccation resistance have a connection to the melanization pathway and multilayer reflectors (60-63). In the subgenus *Catonebria*, which includes the *N. ingens* complex, metallic color variation has been gained and lost many times with a general trend that metallic species occur in cooler and wetter regions compared to related species with darker, less or non-metallic cuticle. For example, among species of the *gebleri* species complex (Kavanaugh et al. 2021), those from more northern and coastal regions (northern Cascade Range and northern Rocky Mountains; namely, *Nebria gebler*i Dejean and *Nebria cascadensis* Kavananugh) are more vividly metallic than those from the Sierra Nevada and other southern ranges in California (i.e., *Nebria albimontis* Kavanaugh, *Nebria rathvoni* LeConte, and *Nebria siskiyouensis* Kavanaugh). The same general pattern is seen among members of the *meanyi* species complex as well as in other closely related *Nebria* subgenera. To investigate this phenomenon, we explored the possibility that metallic variation might be associated with water availability in *N. ingens* habitats, with the expectation that the black species (loss of metallic color) could have higher fitness in drier and warmer habitats. Evidence from other beetle species has shown a relationship between the *yellow* gene, cuticle melanization, and water retention ability (42). This leads to the hypothesis that the loss of metallic color, as a byproduct of melanin accumulation, is the result of adaptation to arid environments. Our result of a correlation between color and water loss rate supports this hypothesis. Furthermore, the significant positive correlation

between metallic color variation and water availability (SWE) in the environment indicates that black beetles are more frequently found in the drier and warmer southern Sierra Nevada. If metallic color is responsive to local environmental adaptation, we would expect to see a signature of selection for genes involved in metallic coloration.

From an evolutionary perspective, metallic color variation in beetles, to our knowledge, has not been reported as a driver or reinforcer of speciation despite its prevalence in many closely related taxa. In the *N. ingens* complex, we found that alleles of the *yellow*-like gene are maintained in each species despite gene flow, forming a genomic island of divergence in the genomic landscape (**Figure 4**). Genomic islands of divergence may drive or reinforce reproductive isolation in this species complex, although we note that this is not through assortative mating (26). An alternative explanation is that local adaptation to the heterogeneous environments of the northern and southern Sierra Nevada (e.g., water availability) has maintained this phenotype despite admixture during glacial episodes (26). A next step will be to develop direct evidence from fitness experiments of different color forms and their offspring to further strengthen these inferences.

Materials and Methods

Animal, genotyping, and color variation

Adult beetles of the *N. ingens* complex (n=383) were collected from 27 populations, encompassing the entire distribution range of the species complex (**Figure 1**). Whole-genome resequencing data from 374 beetles were generated in our previous study using the GATK variant calling pipeline (52). After removing samples lacking color phenotype data, we performed GWAS using a SNP matrix with 355 beetles and 1,237,702 SNPs. To quantify color variation, we measured the reflectance spectra from the elytral surface of 368 beetles using a hyperspectral camera (Specim IQ). The average spectrum was measured from each pixel in the brightest elytral region (8-600 pixels, median=190 pixels) to represent the individual reflectance spectrum. The mean reflectance spectrum was then used to calculate the CIELAB color space for each elytron (53) using the CIE standard illuminant D65 with a custom MATLAB script, in which we used axis a* (the green-red axis) to represent the color of the elytra.

Cuticular structure of the metallic hue

The elytra of three beetles, representing *N. ingens*, *N. riversi*, and a genetically admixed hybrid lineage, were used to examine the cuticular microstructure with transmission electron microscopy (TEM). We used a FEI Tecnai T12 microscope in the School of Medicine and Public Health at UW-Madison. The samples were stored in -20°C with 95% ethanol before use. The images with clear structure were selected to measure the thickness of each that composed the epicuticle. We took 13-30 vertical transects to repeat measurements of thickness for each specimen using ImageJ (54). Counts of layers and their thickness were used to predict the reflectance spectra of each specimen using a multilayer reflectance calculator provided by Co. Filmetrics®, with the refractive indices of electron dense and electron lucent being 1.7 and 1.4, respectively. These indices are consistent across different beetle taxa (6, 55). The calculated reflectance spectrum was subsequently used to compare with the observed spectra from the same individual beetle, except for the green elytrum for which we compared the calculated spectrum to other bright green beetles from the same population, to verify the source of the metallic color.

Genome-wide association mapping

To identify SNP markers associated with the color phenotype, we performed GWAS using latent factor mixed models (LFMM) (56). Ten latent factors were specified to account for population structure, which includes a pattern of isolation by distance across seven ancestral population clusters (Weng et al., 2021). The regularized least squares estimate of causal variants were obtained using both ridge and lasso regression. To reduce the false-discovery rate (FDR), we first calibrated the *p* values with genomic inflation factors (GIF), then adjusted the calibrated *p* values using the Benjamini-Hochberg multiple-testing procedure at an adjusted *p* value at 0.001. SNPs that passed the significance level in both ridge and lasso regression were used to find the intersecting genes from the published genome using bedtools v2.28 (57, 58). For each of the candidate genes, we calculated the number of candidate SNPs and the mean *p* values of all SNPs. We then conducted GO-term enrichment analysis to detect the functional enrichment of gene

pathways for each trait, using the R package clusterProfiler v.3.16.1 with a p value ≤ 0.001 (Yu *et al.* 2012). Redundant GO terms were collapsed and summarized using REVIGO (Supek *et al.* 2011), relative to the UniProt database of *Drosophila melanogaster* (7227, accessed November 8, 2021).

Genetic divergence of color candidate genes

To assess genetic divergence patterns of five candidate color-associated genes, we extracted the SNPs to calculate population pairwise F_{ST} for each gene, as well as the genome-wide intragenic and intergenic regions separately, using vcftools (59). We calculated these values for all 22 populations that contained more than five individuals. High values of F_{ST} were determined after subtracting genome-wide intragenic F_{ST} for the five candidate genes ($F_{ST(candidate)}$ - $F_{ST(intragenic)}$). In addition, we also subtracted intergenic F_{ST} from intragenic F_{ST} to observe a general pattern of elevated F_{ST} in the putatively selected regions. The pairwise F_{ST} was visualized on a map of sampled populations (**Figure 4**).

Since the *yellow*-like gene has elevated F_{ST} (higher than the overall intragenic regions) almost exclusively between the populations across the historical contact zone (the San Joaquin Basin), we further assessed the extremeness of this pattern for the *yellow*-like gene. Specifically, we calculated the contact zone-specific F_{ST} (defined by mean of pairwise $F_{ST(contact\text{-}zone,\ interspecific\ pairs)}$ - mean of pairwise $F_{ST(all\ other\ pairs)}$) for all genes with SNPs and for all genes with more than 50 SNPs (**Figure 4B**). We excluded genes with 50 or fewer SNPs to avoid the extremes that arise from a small number of linked SNPs in relatively small genes (**Figure S5**). For the 2,186 genes with more than 50 SNPs including the *yellow*-like gene, we used the distribution of contact zone-specific F_{ST} to assess the extremeness of the *yellow*-like gene (**Figure 4B**).

Testing for environmental selection on color variation

Because color variation is a key diagnostic character separating two species in the *N. ingens* complex (**Figure 1**), it may be associated with adaptation to local environments (26, 60). We investigated the correlation between color variation, water loss rate of beetles,

and the snow water equivalent (SWE) in the habitats of the sampled populations. To quantify the water loss rate, 87 beetles were placed individually in a tube in a sealed container, which contained lithium chloride (LiCl) as a desiccant to maintain a relative humidity between 20 and 30 percent. The temperature was controlled at 5°C during the experiment, which is similar to the natural foraging temperature in the field. The water loss rate was calculated by weighing beetles before and after 24 hours of desiccation. SWE data were extracted from published Sierra Nevada snow analysis results using the R package raster v3.6-3 (61, 62). Spearman's rank correlation coefficient (ρ) was used to assess the correlation since the data were non-normal in distribution.

Acknowledgments

We thank Filmetrics® for granting permission to use the reflectance calculator. We thank the National Parks of the United States, including Yosemite, Sequoia and Kings Canyon National Parks, for providing permission to conduct research in the parks. This research was financially supported by the Valentine Eastern Sierra Reserve (UC Santa Barbara Natural Reserve System) through VESR Graduate Student Funding and the Ministry of Education of the Republic of China (Taiwan) through the Government Scholarship to Study Abroad to Y.M.W. We thank the PhD committee of Y.M.W., consisting of Daniel Young, Carol Lee, Prashant Sharma, and Jun Zhu, for providing suggestions regarding this study. The authors have no conflicts of interests to declare.

Author Contributions: YMW, DHK, and SDS developed the original idea; YMW and SDS designed the experiments. The quantification of color variation was conducted by YMW, BRP, and JS and other analyses were performed by YMW. YMW and SDS wrote the first draft of the manuscript and DHK, BRP, JS, and MAK provided comments to improve the manuscript.

References

1. B. C. Ratcliffe, Scarab Beetles in Human Culture. *The Coleopterists Bulletin* **60**, 85-101, 117 (2006).

2. V. Z. Rivers, Emeralds on wing: Jewel beetles in textiles and adornment. *Insects" in oral literature and traditions* (2003).
3. A. E. Seago, P. Brady, J. P. Vigneron, T. D. Schultz, Gold bugs and beyond: a review of iridescence and structural colour mechanisms in beetles (Coleoptera). *J R Soc Interface* **6 Suppl 2**, S165-184 (2009).
4. S. O. Andersen, "Chapter 94 - Exoskeleton" in Encyclopedia of Insects (Second Edition), V. H. Resh, R. T. Cardé, Eds. (Academic Press, San Diego, 2009), pp. 339-342.
5. M. A. Barry *et al.*, Evolutionary algorithms converge towards evolved biological photonic structures. *Scientific Reports* **10**, 12024 (2020).
6. M. Kurachi, Y. Takaku, Y. Komiya, T. Hariyama, The origin of extensive colour polymorphism in *Plateumaris sericea* (Chrysomelidae, Coleoptera). *Naturwissenschaften* **89**, 295-298 (2002).
7. L. P. Biró, J. P. Vigneron, Photonic nanoarchitectures in butterflies and beetles: valuable sources for bioinspiration. *Laser & Photonics Reviews* **5**, 27-51 (2011).
8. E. Colusso *et al.*, Bioinspired stimuli-responsive multilayer film made of silk–titanate nanocomposites. *Journal of Materials Chemistry C* **5**, 3924-3931 (2017).
9. L. Biró *et al.*, Bioinspired artificial photonic nanoarchitecture using the elytron of the beetle Trigonophorus rothschildi varians as a 'blueprint'. *Journal of the Royal Society Interface* **7**, 887-894 (2010).
10. L. R. Strickland *et al.*, Inheritance, distribution and genetic differentiation of a color polymorphism in Panamanian populations of the tortoise beetle, Chelymorpha alternans (Coleoptera: Chrysomelidae). *Heredity (Edinb)* **122**, 558-569 (2019).
11. M. V. Kozlov *et al.*, Climate shapes the spatiotemporal variation in color morph diversity and composition across the distribution range of *Chrysomela lapponica* leaf beetle. *Insect Science* **29**, 942-955 (2022).
12. S. Fujiyama, K. Arimoto, "Genetics of the two colour forms of Chrysolina aurichalcea (Mannerheim)(Coleoptera: Chrysomelidae) and their gene frequencies in two mountainous areas of central Honshu, Japan" in Biology of chrysomelidae. (Springer, 1988), pp. 205-215.
13. W. Paarmann, T. Assmann, D. Mossakowski, W. Rohe, I. Lüchtrath (2007) Heredity of the elytral colour in adults of Poecilus lepidus Leske (Coleoptera, Carabidae). in *Proceedings of the 13th European Carabidologists' Meeting, Blagoevgrad*, pp 183-194.
14. M. E. Favila, G. Ruiz-Lizarraga, J. Nolasco, Inheritance of a red cuticular color mutation in the scarab beetle Canthon cyanellus cyanellus LeConte (Coleoptera: Scarabaeidae). *The Coleopterists Bulletin* **54**, 541-546 (2000).
15. J. Vasconcellos-Neto, "Genetics of Chelymorpha cribraria, Cassidinae: colour patterns and their ecological meanings" in Biology of Chrysomelidae. (Springer, 1988), pp. 217-232.
16. H. Gotoh, L. C. Lavine, Genetic control of color polymorphism in the stag beetle Cyclommatus metallifer boisduval (Coleoptera: Lucanidae). *The Coleopterists Bulletin* **68**, 209-214 (2014).
17. A. L. V. DAVIS, D. J. BRINK, C. H. SCHOLTZ, L. C. PRINSLOO, C. M. DESCHODT, Functional implications of temperature-correlated colour polymorphism in an iridescent, scarabaeine dung beetle. *Ecological Entomology* **33**, 771-779 (2008).

18. L. Zhang, A. Mazo-Vargas, R. D. Reed, Single master regulatory gene coordinates the evolution and development of butterfly color and iridescence. *Proceedings of the National Academy of Sciences* **114**, 10707-10712 (2017).
19. A. Prakash, C. Finet, T. D. Banerjee, V. Saranathan, A. Monteiro, Antennapedia and optix regulate metallic silver wing scale development and cell shape in *Bicyclus anynana* butterflies. *Cell Reports* **40**, 111052 (2022).
20. J. W. Galusha, L. R. Richey, J. S. Gardner, J. N. Cha, M. H. Bartl, Discovery of a diamond-based photonic crystal structure in beetle scales. *Physical Review E. covering statistical, nonlinear, biological, and soft matter physics* **77**, 050904 (2008).
21. S. Luke, P. Vukusic, "Amorphous Nanophotonics in Nature" in Amorphous Nanophotonics*,* C. Rockstuhl, T. Scharf, Eds. (Springer Berlin Heidelberg, Berlin, Heidelberg, 2013), pp. 267-287.
22. J. F. Colomer *et al.*, Photonic polycrystal in the greenish-white scales of the African longhorn beetle *Prosopocera lactator* (Cerambycidae). *Physical Review E. covering statistical, nonlinear, biological, and soft matter physics* **85**, 011907 (2012).
23. P. Simonis, J. P. Vigneron, Structural color produced by a three-dimensional photonic polycrystal in the scales of a longhorn beetle: *Pseudomyagrus waterhousei* (Coleoptera: Cerambicidae). *Physical Review E. covering statistical, nonlinear, biological, and soft matter physics* **83**, 011908 (2011).
24. A. Ren *et al.*, Convergent evolution of broadband reflectors underlies metallic coloration in butterflies. *Frontiers in Ecology and Evolution*, 206 (2020).
25. S. D. Schoville, G. K. Roderick, D. H. Kavanaugh, Testing the 'Pleistocene species pump'in alpine habitats: lineage diversification of flightless ground beetles (Coleoptera: Carabidae: Nebr*ia) in* relation to altitudinal zonation. *Biological Journal of the Linnean Society* **107**, 95-111 (2012).
26. Y. M. Weng, D. H. Kavanaugh, S. D. Schoville, Drainage basins serve as multiple glacial refugia for alpine habitats in the Sierra Nevada Mountains, California. *Molecular Ecology* **30**, 826-843 (2021).
27. D. Lindtke, S. C. González-Martínez, D. Macaya-Sanz, C. Lexer, Admixture mapping of quantitative traits in Populus hybrid zones: power and limitations. *Heredity (Edinb)* **111**, 474-485 (2013).
28. C. A. Buerkle, C. Lexer, Admixture as the basis for genetic mapping. **23**, 686-694 (2008).
29. A. E. Seago, R. Oberprieler, V. K. Saranathan, Evolution of Insect Iridescence: Origins of Three-Dimensional Photonic Crystals in Weevils (Coleoptera: Curculionoidea). *Integrative and Comparative Biology* **59**, 1664-1672 (2019).
30. J. Lee, T. Terlier, Y. J. Jang, K.-B. Lee, Y. Lee, Structural colors and physical properties of elytra in the jewel beetle, Chrysochroa fulgidissima, using surface analytical techniques. *Surface and Interface Analysis* **52**, 656-664 (2020).
31. A. Luna *et al.*, Characterization of the iridescence-causing multilayer structure of the Ceroglossus suturalis beetle using bio-inspired optimization strategies. *Optics Express* **21**, 19189-19201 (2013).
32. J. M. Pasteels, O. Deparis, S. R. Mouchet, D. M. Windsor, J. Billen, Structural and physical evidence for an endocuticular gold reflector in the tortoise beetle, *Charidotella ambita*. *Arthropod Structure & Development* **45**, 509-518 (2016).
33. J. A. Noyes, P. Vukusic, I. R. Hooper, Experimental method for reliably establishing the refractive index of buprestid beetle exocuticle. *Optics Express* **15**, 4351-4358 (2007).

34. E. Bermúdez-Ureña, C. Kilchoer, N. P. Lord, U. Steiner, B. D. Wilts, Structural diversity with varying disorder enables the multicolored display in the longhorn beetle *Sulawesiella rafaelae*. *iScience* **23**, 101339 (2020).
35. D. Mckenzie, M. Large, Multilayer reflectors in animals using green and gold beetles as contrasting examples. *Lournal of Experimental Biology* **201 (Pt 9)**, 1307-1313 (1998).
36. D. Mossakowski, W. Paarmann, Elytral surface structure in Poecilus lepidus (Coleoptera: Carabidae): What about the nature of its inheritance? *European Journal of Entomology* **111** (2014).
37. R. A. Stanbrook, W. E. Harris, C. P. Wheater, M. Jones, Evidence of phenotypic plasticity along an altitudinal gradient in the dung beetle. *PeerJ* **9**, e10798 (2021).
38. Y. Arakane, M. Y. Noh, T. Asano, K. J. Kramer, "Tyrosine metabolism for insect cuticle pigmentation and sclerotization" in Extracellular composite matrices in arthropods. (Springer, 2016), pp. 165-220.
39. M. Y. Noh, S. Muthukrishnan, K. J. Kramer, Y. Arakane, Cuticle formation and pigmentation in beetles. *Current Opinion in Insect Science* **17**, 1-9 (2016).
40. N. Gompel, B. Prud'homme, P. J. Wittkopp, V. A. Kassner, S. B. Carroll, Chance caught on the wing: cis-regulatory evolution and the origin of pigment patterns in *Drosophila*. *Nature* **433**, 481-487 (2005).
41. J. Li, B. M. Christensen, "Biological function of insect yellow gene family" in Recent advances in entomological research. (Springer, 2011), pp. 121-131.
42. M. Y. Noh *et al.*, Loss of function of the yellow-e gene causes dehydration-induced mortality of adult *Tribolium castaneum*. *Developmental Biology* **399**, 315-324 (2015).
43. Y. Zhang *et al.*, Three Melanin Pathway Genes, TH, yellow, and aaNAT, Regulate Pigmentation in the Twin-Spotted Assassin Bug, *Platymeris biguttatus* (Linnaeus). *International Journal of Molecular Sciences* **20** (2019).
44. L. Zhang *et al.*, Genetic Basis of Melanin Pigmentation in Butterfly Wings. *Genetics* **205**, 1537-1550 (2017).
45. M. Ashida, P. T. Brey, Role of the integument in insect defense: pro-phenol oxidase cascade in the cuticular matrix. *Proceedings of the National Academy of Sciences* **92**, 10698-10702 (1995).
46. I. González-Santoyo, A. Córdoba-Aguilar, Phenoloxidase: a key component of the insect immune system. *Entomologia Experimentalis et Applicata* **142**, 1-16 (2012).
47. R. E. Nelson *et al.*, Peroxidasin: a novel enzyme-matrix protein of *Drosophila* development. *EMBO Journal* **13**, 3438-3447 (1994).
48. C. P. Ma, Z. M. Guo, F. L. Zhang, J. Y. Su, Molecular identification, expression and function analysis of peroxidasin in *Chilo suppressalis*. *Insect Science* **27**, 1173-1185 (2020).
49. H. Kan *et al.*, Molecular control of phenoloxidase-induced melanin synthesis in an insect. *Journal of Biological Chemistry* **283**, 25316-25323 (2008).
50. Y. Masuoka, K. Maekawa, Ecdysone signaling regulates soldier-specific cuticular pigmentation in the termite Zootermopsis nevadensis. *FEBS letters* **590**, 1694-1703 (2016).
51. Y. Arakane, S. Muthukrishnan, R. W. Beeman, M. R. Kanost, K. J. Kramer, Laccase 2 is the phenoloxidase gene required for beetle cuticle tanning. *Proceedings of the National Academy of Sciences* **102**, 11337-11342 (2005).

52. W. Yi-Ming, H. K. David, L. R. Peter, P. Gilia, D. S. Sean, Evidence for admixture and rapid evolution during glacial climate change in an alpine specialist. *bioRxiv*, 2023.2009.2021.558886 (2023).
53. A. R. Robertson, The CIE 1976 color-difference formulae. *Color Research & Application* **2**, 7-11 (1977).
54. C. A. Schneider, W. S. Rasband, K. W. Eliceiri, NIH Image to ImageJ: 25 years of image analysis. *Nature Methods* **9**, 671-675 (2012).
55. G. D. Bernard, W. H. Miller, Interference filters in the corneas of Diptera. *Investigative Ophthalmology & Visual Science* **7**, 416-434 (1968).
56. K. Caye, B. Jumentier, J. Lepeule, O. François, LFMM 2: Fast and Accurate Inference of Gene-Environment Associations in Genome-Wide Studies. *Molecular Biology and Evolution* **36**, 852-860 (2019).
57. A. R. Quinlan, I. M. Hall, BEDTools: a flexible suite of utilities for comparing genomic features. *Bioinformatics* **26**, 841-842 (2010).
58. Y. M. Weng, C. B. Francoeur, C. R. Currie, D. H. Kavanaugh, S. D. Schoville, A high-quality carabid genome assembly provides insights into beetle genome evolution and cold adaptation. *Molecular Ecology Resources* **21**, 2145-2165 (2021).
59. P. Danecek *et al.*, The variant call format and VCFtools. *Bioinformatics* **27**, 2156-2158 (2011).
60. E. Van Dyke, Studies on western North American Carabinae (Coleoptera) with descriptions of new species. *The Pan-Pacific entomologist* **1**, 111-125 (1925).
61. R. J. Hijmans, J. van Etten, raster: Geographic analysis and modeling with raster data. R package version 2.0-12. (2012).
62. S. A. Margulis, G. Cortés, M. Girotto, M. Durand, A Landsat-Era Sierra Nevada Snow Reanalysis (1985–2015). *Journal of Hydrometeorology* **17**, 1203-1221 (2016).

Figures and Tables

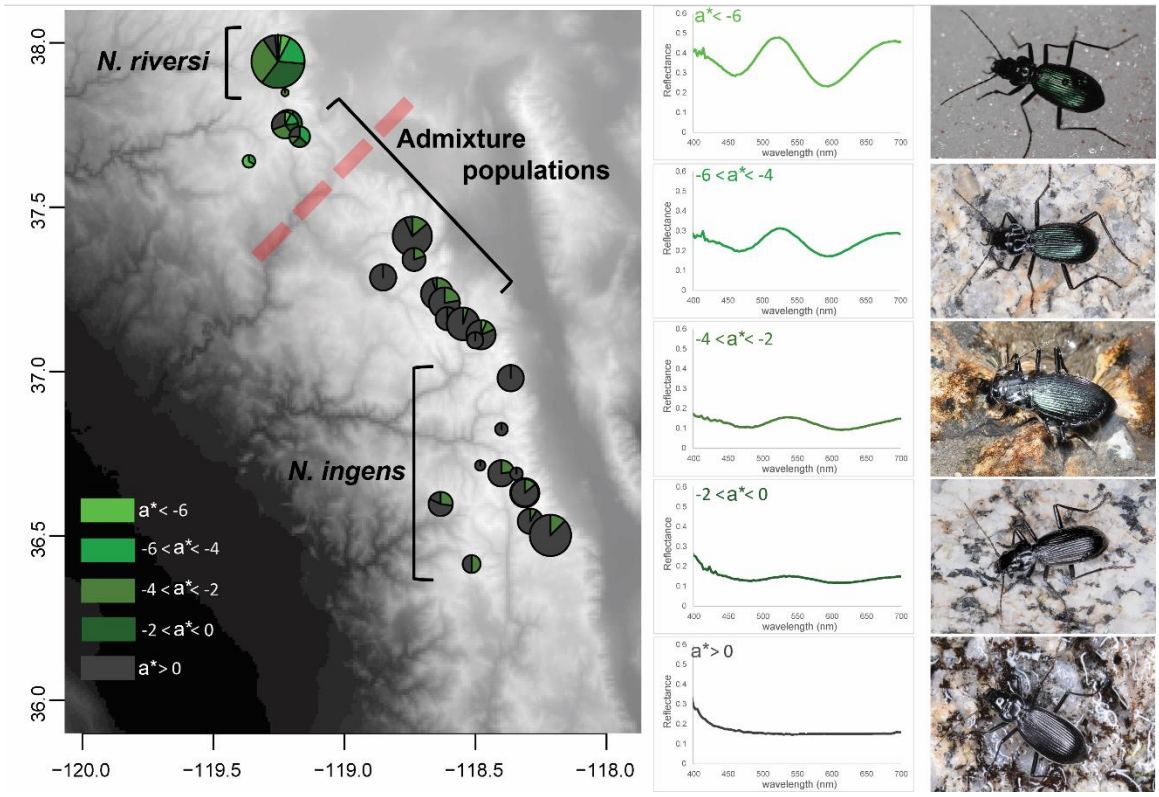

Figure 1. Color variation of the elytra in the *Nebria ingens* species complex. Color is quantified for color space a* (the green-red axis), with negative values indicating the degree of greenness. The left panel shows the geographical distribution of the color variation per site, with the current geographical barrier (San Joaquin Basin, also the historical contact zone) in red dashed line, the middle panel provides examples of the reflection spectrum of individual beetles with different phenotypes, and the right panel shows the photo of beetles roughly corresponding to the reflection spectrum in the middle panel.

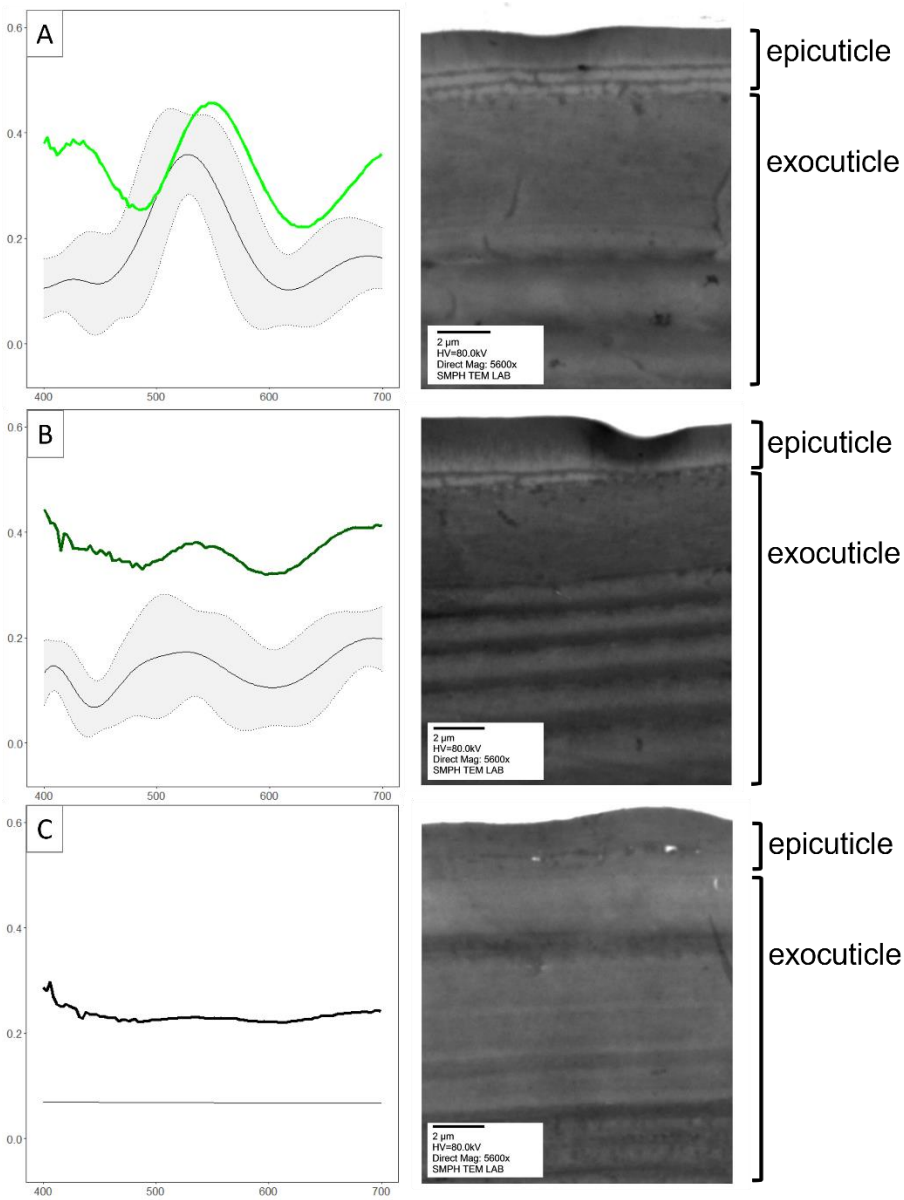

Figure 2. Comparisons of modeled spectra calculated from measurements of the multilayer reflectors in the epicuticle (thin lines represent the mean and the grey area shows the 95% confidence interval) and the observed spectra (colored thick lines) for a set of individuals (except for the green beetle for which we used another beetle from the same population showing the same green light reflection). The TEM images in each spectrum demonstrate the pattern of multilayer reflectors in the epicuticle. The amplitude is not considered in the model as the wavelength is independent from the strength of the light source and would not affect the color space calculation.

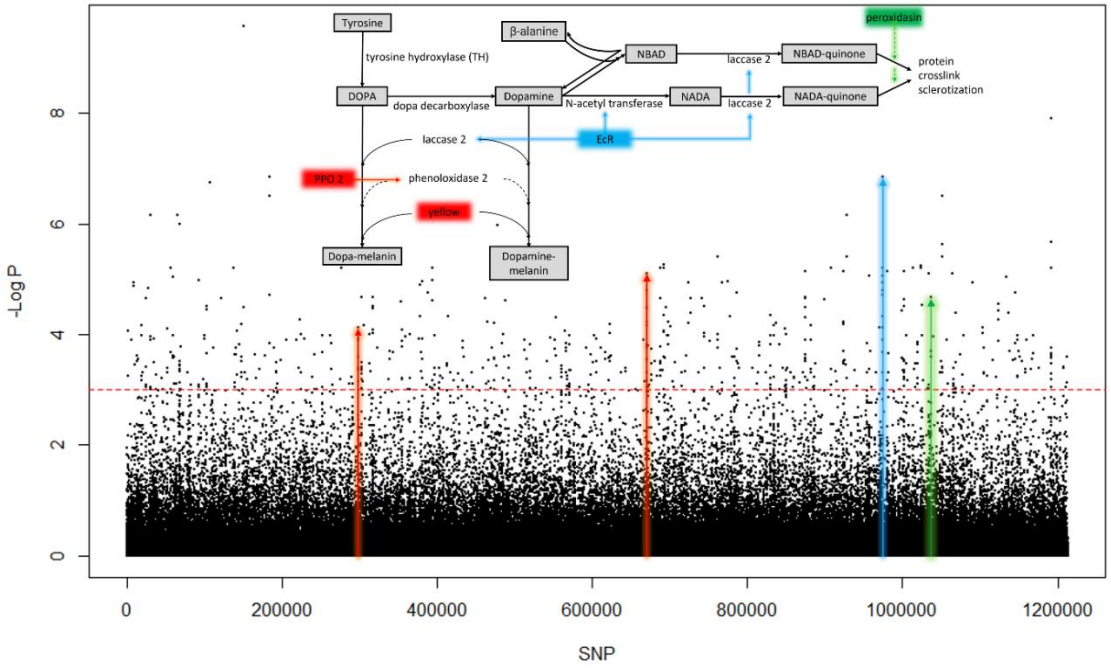

Figure 3. The genome-wide Manhattan plot showing ridge corrected candidate variants identified by LFMM. The red horizontal line defines the Benjamini Hochberg adjusted p-value at 0.001. The red vertical arrows show the genomic position of melanin associated genes including PPO2 and *yellow*-like, while the blue vertical arrow shows the two EcR genes and the green arrow shows the *peroxidasin* gene. The flowchart on the top shows the tyrosine hydroxylase pathway and how the function of each candidate gene putatively affects the cuticle pigmentation. The tyrosine hydroxylase pathway was modified from (39) and (38).

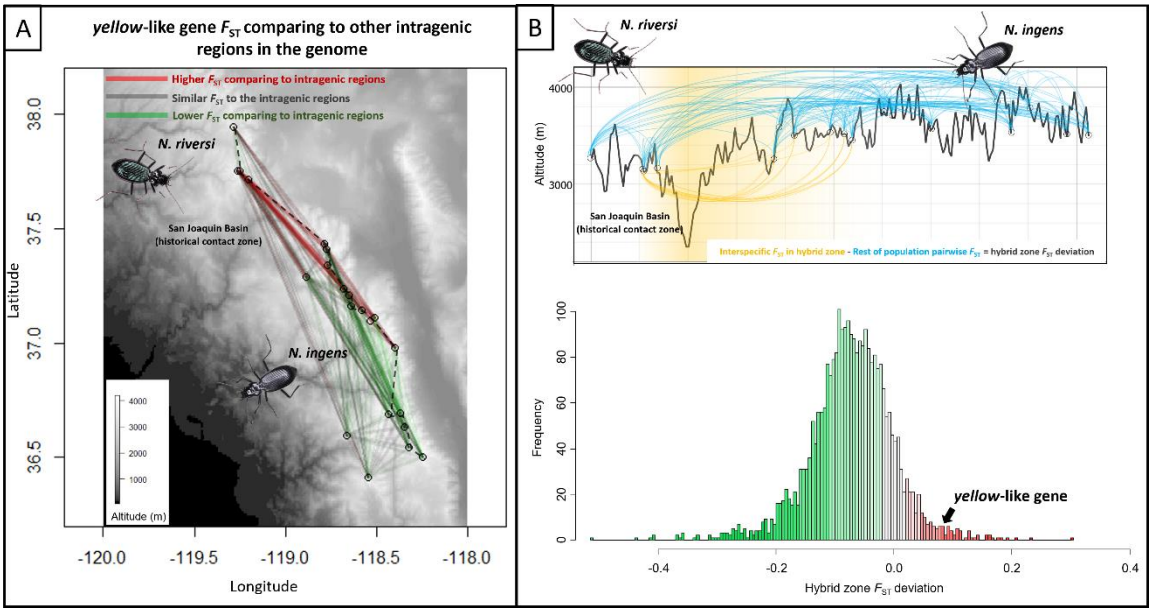

Figure 4. The pattern of elevated F_{ST} for the *yellow*-like gene comparing to the intragenic regions in the genome and other genes. (A) The map shows the population pairwise F_{ST} for the *yellow*-like gene comparing to the genome-wide intragenic regions in the genome, where the thicker lines reflect greater gene flow estimated from putatively neutral regions (1- $F_{ST(intergenic)}$), and the warmer color (red) shows higher F_{ST} of the *yellow*-like gene ($F_{ST(yellow)}$ - $F_{ST(intragenic)}$) compared to the rest of intragenic regions while receding F_{ST} is shown in greener lines. The red thick lines between populations across the San Joaquin Basin (historical contact zone) demonstrate the elevated divergence of *yellow*-like gene comparing with the genome-wide intragenic regions, in the context of low genome-wide interspecific divergence due to the hybridization. (B) For each gene, we calculated the mean of pairwise F_{ST} between interspecific populations in the contact zone (orange lines on the top graph) and subtracted it by that of the rest of population pairs (blue lines, including interspecific and intraspecific comparisons) to assess extremeness of elevated F_{ST} for the *yellow*-like gene in the contact zone. The black thick line depicts the elevation profile from the transacted dash line in (A), and the contact zone is highlighted in the orange cloud. By comparing with another 2,186 genes containing more than 50 SNPs (bottom graph), the *yellow*-like gene has higher exceeding contact zone F_{ST} (0.075) than 98.1% of the other genes (mostly negative, likely due to the historical hybridization event). The comparative F_{ST} of other candidate genes is shown in **Figure S3**.

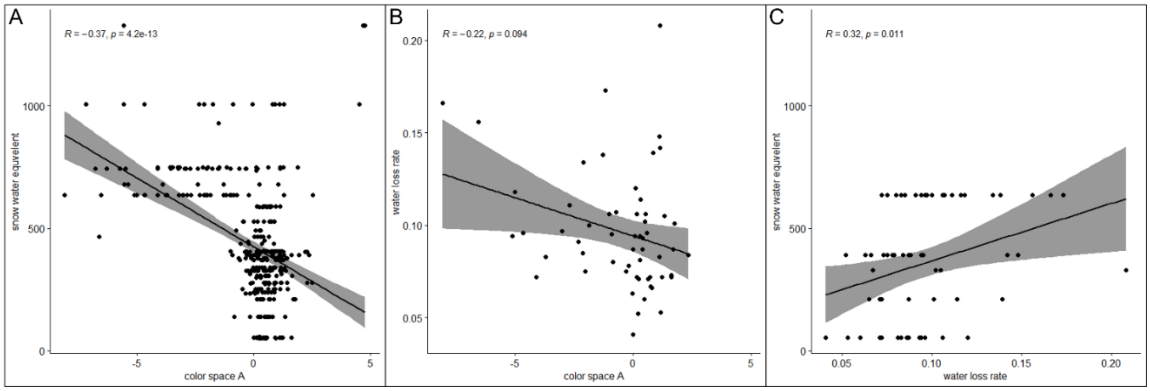

Figure 5. The correlations among elytral color (color space a*), water loss rate, and mean September SWE in the habitat of the *N. ingens* complex. The correlations were calculated with Spearman's rank correlation coefficient and the grey areas show the 95% confidence interval of the estimate. The correlations are significant, except for the color and the water loss rate correlation which has confidence interval overlapping zero (-0.477 to 0.035).

Table 1. The enriched biological process gene ontology (GO) terms from the candidate genes and the genes contributing to each of the term.

GO term	Biological process	Involved candidate genes
GO:0006452	translational frameshifting	eIF5A/VAT1
GO:0048065	male courtship behavior, veined wing extension	Ttgn1/TTYH/USP31
GO:0051046	regulation of secretion	NLGN1/rapgef4 and other 12 genes
GO:0050808	synapse organization	zig-8/NLGN4X and other 6 genes
GO:0033627	cell adhesion mediated by integrin	LOC109622862/αPS2
GO:0098609	cell-cell adhesion	NLGN1/NLGN4X and other 6 genes
GO:0007564	regulation of chitin-based cuticle tanning	TTYH/USP31
GO:0045901	positive regulation of translational elongation	eIF5A/VAT1
GO:0032275	luteinizing hormone secretion	SMG1/TMF
GO:0046879	hormone secretion	rapgef4/SMG1/TMF
GO:0032274	gonadotropin secretion	SMG1/TMF
GO:0060986	endocrine hormone secretion	SMG1/TMF
GO:0048082	regulation of adult chitin-containing cuticle pigmentation	TTYH/USP31
GO:0048079	regulation of cuticle pigmentation	TTYH/USP31
GO:0007449	proximal/distal pattern formation, imaginal disc	vg/vn/Dll
GO:0072583	clathrin-dependent endocytosis	NLGN1/NLGN4X/INPP5F/NA
GO:0031509	subtelomeric heterochromatin assembly	Dot1l/Ptp99A
GO:0010737	protein kinase A signaling	Hemicentin-1/LOC109622862
GO:0042438	melanin biosynthetic process	TTYH/USP31/yellow/PPO2
GO:0044550	secondary metabolite biosynthetic process	TTYH/USP31/yellow/PPO2
GO:0046189	phenol-containing compound biosynthetic process	TTYH/USP31/yellow/PPO2
GO:0006583	melanin biosynthetic process from tyrosine	TTYH/USP31
GO:0035120	post-embryonic appendage morphogenesis	vg/vn/LOC109622862/ds/αPS2/Dll
GO:0007476	imaginal disc-derived wing morphogenesis	vg/vn/LOC109622862/ds/αPS2
GO:0048737	imaginal disc-derived appendage development	vg/vn
GO:0035114	imaginal disc-derived appendage morphogenesis	vg/vn/LOC109622862/ds/αPS2/Dll
GO:0010642	negative regulation of platelet-derived growth factor receptor signaling pathway	ApoD/HGS
GO:0035076	ecdysone receptor-mediated signaling pathway	EcRX1/EcR
GO:0006813	potassium ion transport	LOC108566252/twk-7/TRP/TRP/Kv3